Macromodeling of Multilayered Power Distribution Networks Based on Multiconductor Transmission Line Approach

Sourajeet Roy, *Student Member, IEEE*, and Anestis Dounavis, *Member, IEEE*

***Abstract*— Typical modeling algorithms for multilayered irregular shaped power distribution networks are based on a finite difference solution of the Helmholtz equation. In this paper, the finite difference solution is demonstrated to be equivalent to a discretization of the Telegraphers partial differential equations for multiconductor transmission lines (MTL). With this concept, an efficient macromodeling algorithm for multilayered structures based on MTL theory is presented. The electromagnetic coupling between the plane layers due to wraparound currents is captured by the inductive and capacitive coupling between the multiconductor lines. A delay extraction-based macromodel is used to represent the MTL in SPICE that can better capture the distributed effects of the structure than existing lumped models. This approach is successfully implemented for multilayered structures with irregular geometries and is shown to be more accurate and efficient compared with existing SPICE lumped models.**

***Index Terms*— Delay extraction, dispersion, power distribution networks (PDN), simultaneous switching noise, skin effect, transmission lines, wraparound current.**

I. Introduction

POWER distribution networks (PDN) at the board level directs power from the voltage regulated module (VRM) to the integrated circuits (ICs) and I/O drivers of high speed digital systems [1]. With the progressive increase in clock speed, scaling of supply voltage, high switching speed of logic circuits, and reduced noise margins, effects like ground bounce, electromagnetic interference (EMI), and simultaneous switching noise (SSN) arising in the PDNs can result in undesirable voltage fluctuations propagating over the board and package and lead to significant electromagnetic compatibility (EMC) and signal integrity (SI) issues for high speed packages [1]–[5].

Traditionally, the electric performance of PDNs has been studied using the numerical techniques like finite difference time domain (FDTD) [5]–[7], method of moments (MoMs) [8], finite element method (FEM) [9], and partial element equivalent circuit (PEEC) [10], to name a few. Although such full-wave techniques provide high degree of versatility and accuracy, they result in large system of equations that may be computationally prohibitive for efficient characterization of multilayered PDN structures. An alternative methodology for modeling PDN structures is based on deriving equivalent circuit models that can be easily solved using commercial circuit simulators with IC emphasis like SPICE [11]–[20]. These equivalent circuit models are typically obtained by discretizing power/ground plane pairs into a mesh of transmission line segments assuming a quasi-transverse electromagnetic (quasi-TEM) mode of propagation [15]–[20]. Various SPICE models have been used to represent these transmission line segments such as the conventional lumped model [15]–[17], W-element [19], and delay extraction-based passive compact transmission line (DEPACT) model [20]. However, these models are limited to either single-layered PDNs or multilayered PDNs where the electromagnetic (EM) coupling between the plane layers due to wraparound current has been neglected.

Realistic multilayered PDN designs consist of multiple irregular shaped planes stacked vertically [4]. Due to the presence of apertures, holes, and irregular geometry of the planes, wraparound currents are supported on the active planes, which lead to the EM coupling between individual planes in the transverse direction [4], [21]. Recent works aimed at quantifying the transverse EM coupling are based on transmission line models for coupling through narrow slots [22] and analytic models based on the Green's function [23]. These models provide a frequency domain solution only and may need an additional post processing like rational curve fitting with passivity enforcement [24]–[25] or numerical convolution [26] for transient analysis.

Recently, a model based on the multilayered finite difference method (MFDM) was proposed [21]. The MFDM model is particularly attractive because it discretizes the Helmholtz equation governing the noise propagation over the PDN structure to yield an equivalent 3-D lumped circuit model which can be directly realized in SPICE for both frequency and transient analysis. However, the accuracy of PDN models using lumped elements is limited to scenarios where the rise time of the excitation is much higher than the propagation time over the planes [20]. As the frequency of operation increases, to obtain an accurate broadband lumped model, larger number

Manuscript received June 13, 2012; accepted January 20, 2013. Date of publication February 21, 2013; date of current version May 29, 2013. This work was supported in part by the Natural Sciences and Engineering Research Council of Canada, Canada Foundation for Innovation, Canadian Microelectronics Corporation and Ministry of Research and Innovation—Early Research Award. Recommended for publication by Associate Editor J. Tan upon evaluation of reviewers' comments.

The authors are with the Department of Electrical and Computer Engineering, Western University, London, ON N6A 5B9, Canada (e-mail: sroy33@uwo.ca; adounavis@eng.uwo.ca).

Color versions of one or more of the figures in this paper are available online at http://ieeexplore.ieee.org.

Digital Object Identifier 10.1109/TCPMT.2013.2245377

of lumped sections has to be included leading to larger circuit matrices. Moreover, modeling high frequency effects like skin effect and dispersion requires additional lumped elements (e.g., RL/RC ladder networks [27]), which require augmentation of the original circuit matrices and can quickly lead to prohibitively large memory and run-time costs.

This paper demonstrates that the finite difference solution of the Helmholtz equation in [4] and [21] is equivalent to a simple discretization of Telegraphers partial differential equation for multiconductor transmission line (MTL) segments. Using this concept, an efficient macromodeling algorithm for multilayered structures based on MTL theory is presented. The EM coupling between the plane layers due to wraparound currents is captured by the inductive and capacitive coupling between the multiconductor lines. To obtain an equivalent circuit representation of the MTL compatible with the commercial circuit simulators like SPICE, each MTL segment of the proposed model is represented using the DEPACT segmentation model [28], [29]. The DEPACT model, based on a delay extraction methodology is better able to capture the distributed nature of the structure and is consequently more accurate for the same level of discretization of the PDN structure than existing lumped circuit models [20]. Moreover, the DEPACT macromodel is capable of modeling the frequency-dependent parameters including the skin effect losses and dispersive effects as a low-order rational transfer function that can be solved in SPICE for transient analysis based on a recursive convolution approach [30]. Thus, modeling the frequency-dependent parameters does not require any augmentation of the circuit matrices, thereby yielding the significant savings in the run-time costs over the lumped model of [20].

This paper is organized as follows. Section II briefly describes the lumped circuit framework based on the MFDM used to characterize the transverse coupling between planes [21]. Section III presents the proposed MTL model, and numerical examples and conclusions are presented in Sections IV and V, respectively.

II. Characterizing Coupling Between Planes of a Multilayered PDN

To explain the proposed MTL model for the multilayered PDN, this section reviews the lumped circuit framework that is used to characterize the transverse EM coupling between vertically stacked planes based on the MFDM [21].

Considering the illustrative example consisting of four vertically stacked square planes as shown in Fig. 1(a), it is observed that the presence of an aperture in the middle planes will give rise to wraparound currents, thereby leading to EM coupling between all four planes. The coupled four-plane structure can be considered to be made up of two separate multilayered PDN structure consisting of four and two layers as shown in Fig. 1(b). For the multilayered structures of Fig. 1(b), each ith plane assigns the $i+1$th plane below it as its local reference plane. In other words, considering a current on the bottom of the ith plane, the return path for the same current is considered to exist on the top of the $i+1$th plane below.

A common methodology of modeling the multilayered PDNs of Fig. 1(b) is by discretizing the structures into numerous multilayered square unit cells based on a finite difference treatment of the Helmholtz equation [21]. A unit cell of the four-layered PDN section of Fig. 1(b) is shown in Fig. 2(a). The resistive (R_i), inductive (L_i), capacitive (C_i), conductive (G_i), and skin effect loss ($\hat{R}_i$) parameters of each i^{th} plane of the unit cell of Fig. 2(a) with respect to its local reference [$i+1$th plane of the unit cell of Fig. 2(a)] can be described using a quasi-static model provided the dielectric separation between the planes is much smaller compared with the dimensions of the plane [4] as

$$R_i = \frac{2}{\sigma t_i}, \quad C_i(s) = \varepsilon_o \varepsilon_r(s) \frac{l^2}{d_i}, \quad L_i = \mu_o d_i$$
$$G_i(s) = \omega C_i(s) \tan(\delta_i), \quad \hat{R}_i(s) = 2\sqrt{\frac{s\mu_0}{\sigma}} \tag{1}$$

where $s = j2\pi f$ is the Laplace transform variable, f is the instantaneous frequency, ε_o and μ_o are the permittivity and the permeability of free space, respectively, σ is the conductance of the plane material, $\varepsilon_r(s)$ is the relative permittivity of the dielectric as a function of frequency, t_i and d_i are the thickness of the ith plane and the dielectric layer between the ith and $i+1$th planes, respectively, and l is the dimensions of the unit cell.

To obtain an equivalent circuit model of Fig. 2(a) compatible with SPICE, the local reference planes are replaced by a single common ground plane that is taken as the bottommost planes in the stacked structures of Fig. 1(b). As a result, the electrical parameters of each ith plane of the unit cell of Fig. 2(a) with respect to the common ground is obtained by modifying (1) as [21]

$$L_{i,i} = \mu_o \sum_{k=i}^{N-1} d_k$$
$$L_{i,j} = \begin{cases} L_{i,i} & \text{for } i > j \\ L_{j,j} & \text{for } i < j \end{cases} \tag{2}$$

$$C_{i,i}(s) = \begin{cases} \varepsilon_o \varepsilon_r(s) \frac{l^2}{d_{N-1}} & \text{for } i = N-1 \\ 0 & \text{for } i < N-1 \end{cases}$$
$$C_{i,j}(s) = \begin{cases} \varepsilon_o \varepsilon_r(s) \frac{l^2}{d_i} & \text{for } |\mathrm{i}-\mathrm{j}| = 1 \\ 0 & \text{for } |i-j| > 1 \end{cases} \tag{3}$$
$$G_{i,j}(s) = \omega C_{i,j}(s) \tan \delta_i$$

$$R_{i,j} = \begin{cases} R_i & for\ i = j \\ 0 & for\ i \neq j \end{cases}$$
$$\hat{R}_{i,j}(s) = \begin{cases} \hat{R}_i(s) & for\ i = j \\ 0 & for\ i \neq j \end{cases} \tag{4}$$

where $L_{i,j}$, $C_{i,j}$, $G_{i,j}$, $R_{i,j}$ and $\hat{R}_{i,j}$ represent the coupling term between the i^{th} and jth plane, respectively, for $1 \leq i, j \leq N-1$, and N represents the total number of PDN layers (i.e., $N = 4$ for Fig. 2). It is noted that (2) represents the transverse coupling due to the magnetic flux, and (3) represents the transverse coupling due to the electric field through the dielectric. Overall, (2)–(4) provide a generalized quantification of the coupling of any general N layered PDN. Based on the discretization of the Helmholtz equation and (2)–(4), the equivalent lumped π-model representing each unit

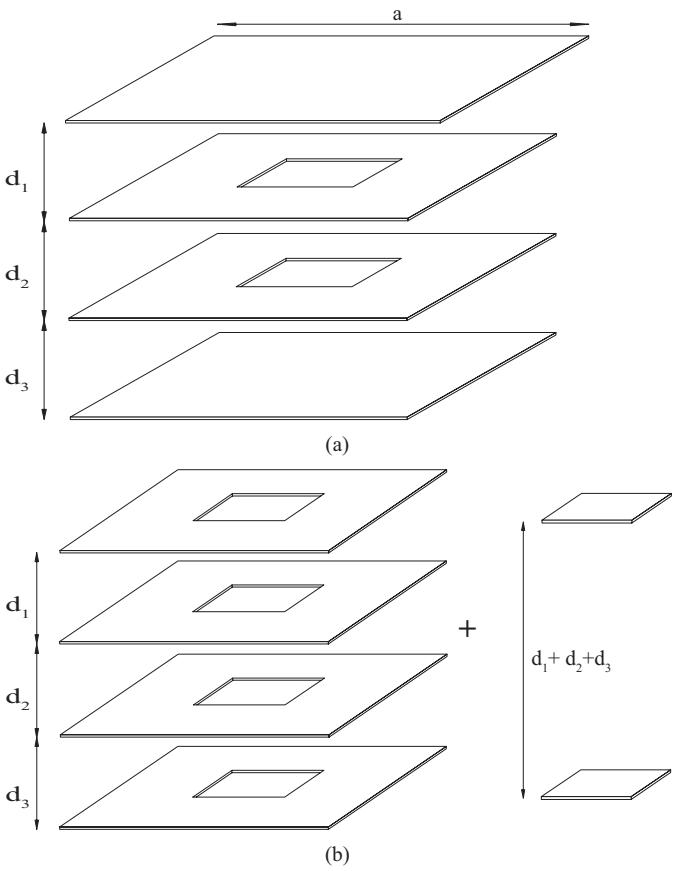

Fig. 1. Illustrative example of multilayered PDN. (a) Original four layered structure. (b) Original structure decomposed into two separate multilayered structures.

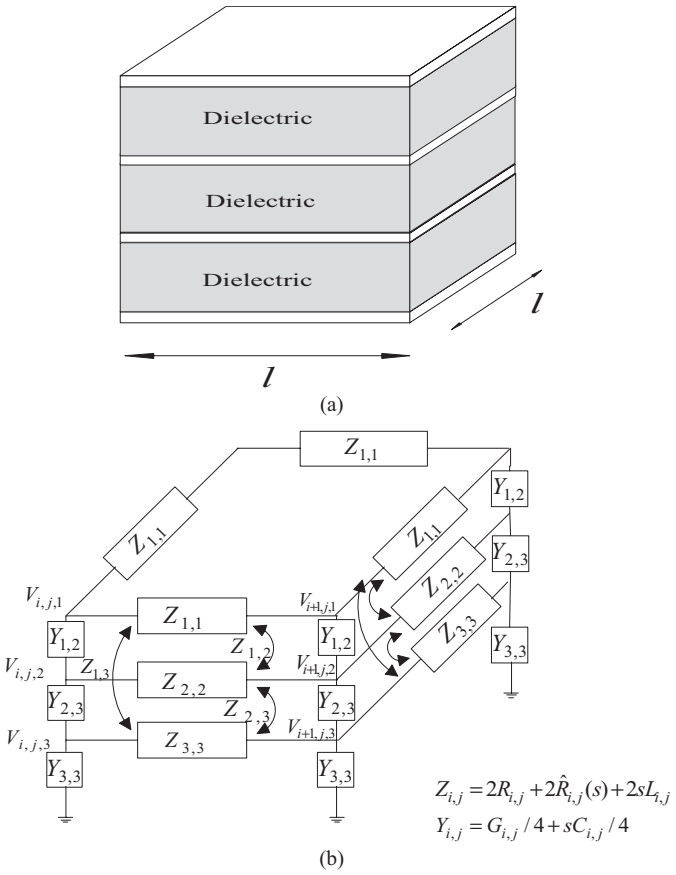

Fig. 2. (a) Unit cell from the four layered PDN of Fig. 1(b). (b) Lumped π model of unit cell.

cell is illustrated in Fig. 2(b) [21]. Each of the frequency-dependent elements of Fig. 2(b) is realized in SPICE using a lumped network [27].

It is noted that the lumped circuit models may require very small discretization (i.e., $l << a$) to capture the distributed effects of the structure, thereby leading to very large modified nodal analysis (MNA) matrices when realized using the commercial circuit simulators like SPICE [20]. Furthermore, realization of the frequency-dependent parameters of (3) and (4) using the lumped circuit elements as proposed in [27] will lead to introduction of additional nodes and further augmentation of the circuit matrices. To address this problem, the proposed distributed MTL model is presented in the following section.

III. Development of Proposed MTL Model

This section begins by demonstrating that the lumped circuit of Fig. 2(b) is equivalent to a simple discretization of the Telegraphers partial differential equations for MTLs. This allows the multilayered structures of Fig. 1(a) to be realized using a mesh of MTLs. Thereafter, the DEPACT macromodel, used to realize the MTL mesh in SPICE, is described.

A. Formulation of the MTL Model

For ease of explanation, the π-model representing any single face of the unit cell of Fig. 2(b) is considered in Fig. 3. The circuit equations governing the voltage/current relationship in the longitudinal direction is given by

$$
\begin{aligned}
V_{i+1,j,k} - V_{i,j,k} = \sum_{m=1}^{N-1} Z_{k,m}\Bigg(& I_{i,j,m}(s) \\
& -\Bigg(\frac{Y_{m-1,m}(s)}{2}\Bigg(V_{i,j,m}(s) + V_{i+1,j,m}(s) - V_{i,j,m-1}(s) \\
& -V_{i+1,j,m-1}(s)) + \frac{Y_{m,m+1}(s)}{2}(V_{i,j,m} + V_{i+1,j,m} \\
& -V_{i,j,m+1}(s) - V_{i+1,j,m-1}(s)\Bigg)\Bigg); \qquad (5) \\
I_{i+1,j,k}(s) - I_{i,j,k}(s) = -\Bigg(\frac{Y_{k-1,k}(s)}{2}(V_{i,j,k}(s) + V_{i+1,j,k}(s) \\
-V_{i,j,k-1}(s) - V_{i+1,j,k-1}(s)) + \frac{Y_{k,k+1}(s)}{2}(V_{i,j,k}(s) \\
+V_{i+1,j,k}(s) - V_{i,j,k+1}(s) - V_{i+1,j,k-1}(s))\Bigg)
\end{aligned}
$$

where the quantities $Z_{k,m}$ and $Y_{k,m}$ for $1 \le k, m \le N-1$ is provided in Fig. 2(b). Defining a new set of variables, $Z_{k,m}^{(\mathrm{pul})} = Z_{k,m}/l$ and $Y_{k,m}^{(\mathrm{pul})} = Y_{k,m}/l$ and replacing them in (5), followed by dividing both sides of (5) by $l$and taking the limit

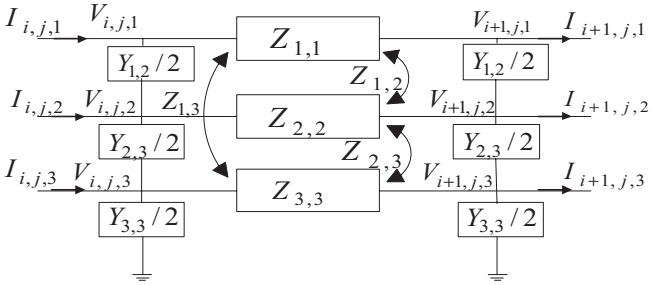

Fig. 3. Lumped circuit of a single face of unit cell.

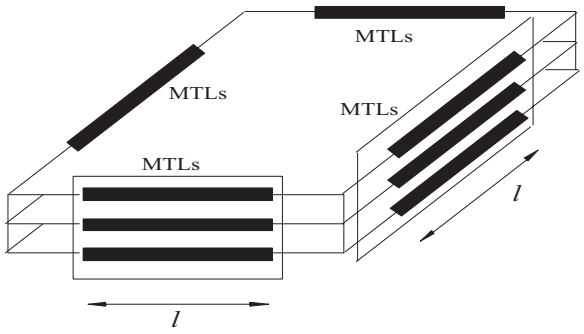

Fig. 4. Unit cell representation using mesh of MTLs.

to $l \to 0$, yields after some algebraic manipulations

$$\lim_{l\to 0}\frac{V_{i+1,j,k}(s)-V_{i,j,k}(s)}{l} = -\sum_{m=1}^{N-1} Z^{(\mathrm{pul})}_{k,m}(s) I_{i,j,m}$$
$$\lim_{l\to 0}\frac{I_{i+1,j,k}(s)-I_{i,j,k}(s)}{l} = -\sum_{m=1}^{N-1} Y^{(\mathrm{pul})}_{k,m}(s) V_{i,j,m}. \tag{6}$$

The left-hand side of (6) represents a spatial differential operator and (6) can be rewritten as the following differential equation as:

$$\frac{\partial}{\partial x}\begin{bmatrix} \boldsymbol{V}_{i,j}(s) \\ \boldsymbol{I}_{i,j}(s) \end{bmatrix} = \begin{bmatrix} 0 & -\mathbf{Z}^{(\mathrm{pul})}(s) \\ -\mathbf{Y}^{(\mathrm{pul})}(s) & 0 \end{bmatrix}\begin{bmatrix} \boldsymbol{V}_{i,j}(s) \\ \boldsymbol{I}_{i,j}(s) \end{bmatrix} \tag{7}$$

where $\boldsymbol{Z}^{(\mathrm{pul})}(s)$ and $\boldsymbol{Y}^{(\mathrm{pul})}(s)$ are the per-unit-length (PUL) impedance and admittance matrices whose entry in the kth row and mth column is $Z^{(\mathrm{pul})}_{k,m}$ and $Y^{(\mathrm{pul})}_{k,m}$, respectively, and the vectors $\boldsymbol{V}_{i,j}(s)$ and $\boldsymbol{I}_{i,j}(s)$ are defined as

$$\boldsymbol{V}_{i,j}(s) = [V_{i,j,1}(s), \ldots, V_{i,j,N-1}(s)]^t$$
$$\boldsymbol{I}_{i,j}(s) = [I_{i,j,1}(s), \ldots, I_{i,j,N-1}(s)]^t. \tag{8}$$

The matrices $\boldsymbol{Z}^{(\mathrm{pul})}(s)$ and $\boldsymbol{Y}^{(\mathrm{pul})}(s)$ are related to the unit cell parameters of (2)–(4) as

$$\boldsymbol{Z}^{(\mathrm{pul})}(s) = \boldsymbol{R}(s) + s\boldsymbol{L}(s)$$
$$\boldsymbol{Y}^{(\mathrm{pul})}(s) = \boldsymbol{G}(s) + s\boldsymbol{C}(s) \tag{9}$$

where

$$R(s)_{k,m} = 2[R_{k,m} + Re(\hat{R}_{k,m}(s))]/l$$
$$L(s)_{k,m} = 2[L_{k,m} + (Im(\hat{R}_{k,m}(s))/s)]/l$$
$$C(s)_{k,m} = [C_{k,m}(s)]/(4l)$$
$$G(s)_{k,m} = [G_{k,m}(s)]/(4l) \tag{10}$$

and $R(s)_{k,m}$, $L(s)_{k,m}$, $C(s)_{k,m}$, and $G(s)_{k,m}$ are the entries in the kth row and mth column of $\boldsymbol{R}(s), \boldsymbol{L}(s), \boldsymbol{C}(s)$, and $\boldsymbol{G}(s)$ matrices, respectively. It is observed that (7) is the general form of the Telegraphers partial differential equation governing the signal propagation in a MTL structure in the frequency domain. With the above discussion, it is appreciated that the finite difference solution of the Helmholtz equation for an unit cell can be represented using distributed MTLs (as shown in Fig. 4) as an alternative to the lumped circuit model derived from MFDM [21]. To obtain an equivalent circuit representation of the MTL compatible with the commercial circuit simulators like SPICE, each MTL segment of the Fig. 4 is modeled using the DEPACT segmentation model [28], [29] as explained in the next subsection.

B. Modeling MTL Segments Using DEPACT

Considering the MTL segment making up each face of the unit cell of Fig. 4 as illustrated in Fig. 5, the solution of (7) can be written as an exponential matrix function [28], [29] as

$$\begin{bmatrix} \boldsymbol{V}_{i+1,j}(s) \\ -\boldsymbol{I}_{i+1,j}(s) \end{bmatrix} = e^{\boldsymbol{\Phi}}\begin{bmatrix} \boldsymbol{V}_{i,j}(s) \\ \boldsymbol{I}_{i,j}(s) \end{bmatrix} \tag{11}$$

where

$$\boldsymbol{\Phi} = \boldsymbol{A}(s) + \boldsymbol{B}(s)$$
$$\boldsymbol{A} = \begin{bmatrix} \mathbf{0} & -\boldsymbol{R}(s) - s(\boldsymbol{L}(s) - \boldsymbol{L}_\infty) \\ -\boldsymbol{G}(s) - s(\boldsymbol{C}(s) - \boldsymbol{C}_\infty) & \mathbf{0} \end{bmatrix} l$$
$$\boldsymbol{B} = \begin{bmatrix} \mathbf{0} & -\boldsymbol{L}_\infty \\ -\boldsymbol{C}_\infty & \mathbf{0} \end{bmatrix} l \tag{12}$$

and $\boldsymbol{L}_\infty = \boldsymbol{L}(s_\infty)$ and $\boldsymbol{C}_\infty = \boldsymbol{C}(s_\infty)$ are the PUL inductive and capacitive parameters of (10) evaluated at the maximum frequency of interest $s_\infty = j2\pi f_{\max}$. Typically, the solution of (11) does not have an exact time domain counterpart and hence segmentation-based modeling techniques [28], [29], [31]–[36] are generally used to derive an equivalent time domain expression of (11). Of these segmentation algorithms, the DEPACT is particularly attractive due to fact that it explicitly extracts the delay of the network leading to better accuracy of the model compared with lumped models of same level of discretization. The basic idea of DEPACT is to extract the delay terms ($e^{s\mathbf{B}}$) from $e^{(\mathbf{A}(s)+s\mathbf{B})}$. However, this is not a trivial task because the matrices $\boldsymbol{A}(s)$ and s$\boldsymbol{B}$ do not commute, (i.e., $e^{(\mathbf{A}(s)+s\mathbf{B})} \neq e^{\mathbf{A}(s)}e^{s\mathbf{B}}$). To approximate $e^{(\mathbf{A}(s)+s\mathbf{B})}$ in terms of a product of exponentials, a modified Lie product [37] is used as

$$e^{\mathbf{A}(s)+s\mathbf{B}} \approx \prod_{i=1}^{n}\boldsymbol{\Psi}_i + \varepsilon_n \text{ and } \boldsymbol{\Psi}_i = e^{\frac{\mathbf{A}(s)}{2n}}e^{\frac{s\mathbf{B}}{n}}e^{\frac{\mathbf{A}(s)}{2n}} \tag{13}$$

where n is the number of sections. Equation (13) provides a methodology of discretizing each MTL section into a cascade of alternating subsections with the individual stamps of $e^{\mathbf{A}/2n}$ and $e^{s\mathbf{B}/n}$ as illustrated in Fig. 5 where $n = 1$ due to the small size of each unit cell [20]. The exponential matrix $e^{\mathbf{A}(s)/2n}$ represents the attenuation losses of the transmission line, whereas the matrix $e^{s\mathbf{B}/n}$ containing only $\boldsymbol{L}_\infty$ and $\boldsymbol{C}_\infty$ represent the delays of the MTL segment.

In Fig. 5, the modeling of the lossless subsections of (13) is performed using a similarity transformation to decouple

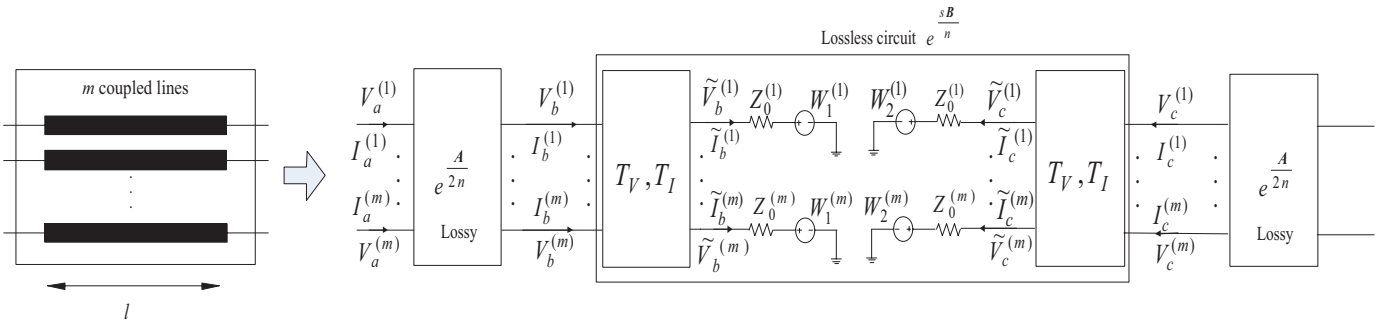

Fig. 5. DEPACT realization of single face of the unit cells using MTLs from Fig. 4.

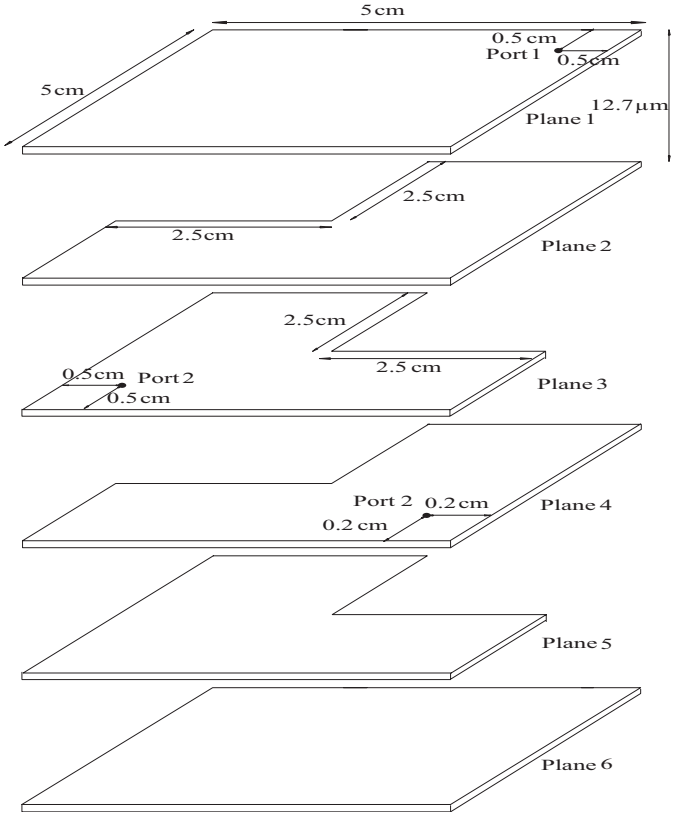

Fig. 6. Test structure for Example 1.

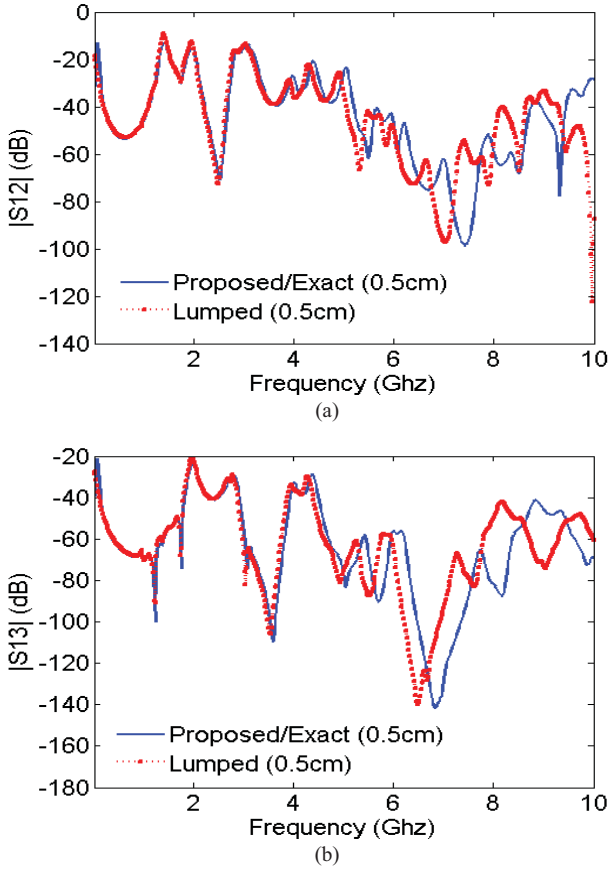

Fig. 7. Comparison of S parameters of Example 1 using proposed and lumped models for cell dimensions $l = 0.5$ cm. (a) Magnitude of S_{12} . (b) Magnitude of S_{13}.

the lossless MTLs into single conductors followed by the MoC algorithm [38], [39]. In [20], a Padé approximation was derived to model the lossy subsections of (13) for single-layered PDNs. In the next section, the methodology to obtain the same Padé approximation for the case of multilayered PDNs is explained.

C. SPICE Realization of Lossy Section

Based on (13), the lossy subsection with the stamp of $e^{\boldsymbol{A}(s)/2}$ (Fig. 5) can be represented as

$$\begin{bmatrix} \boldsymbol{V}_b(s) \\ -\boldsymbol{I}_b(s) \end{bmatrix} = e^{\boldsymbol{A}(s)/2} \begin{bmatrix} \boldsymbol{V}_a(s) \\ \boldsymbol{I}_a(s) \end{bmatrix} = e^{\begin{bmatrix} \boldsymbol{0} & -\boldsymbol{Z}(s) \\ -\boldsymbol{Y}(s) & \boldsymbol{0} \end{bmatrix} l} \begin{bmatrix} \boldsymbol{V}_a(s) \\ \boldsymbol{I}_a(s) \end{bmatrix}. \tag{14}$$

The variables $\boldsymbol{V}_a(s), \boldsymbol{I}_a(s), \boldsymbol{V}_b(s)$, and $\boldsymbol{I}_b(s)$ represent the near and far end voltage and current variable vectors as illustrated in Fig. 5, respectively, and

$$\boldsymbol{Z}(s) = \frac{\boldsymbol{R}(s) + s(\boldsymbol{L}(s) - \boldsymbol{L}_\infty)}{2}$$
$$\boldsymbol{Y}(s) = \frac{\boldsymbol{G}(s) + s(\boldsymbol{C}(s) - \boldsymbol{C}_\infty)}{2}. \tag{15}$$

To capture the frequency dependence of the parameters of (14), the functions of (15) are approximated as a rational

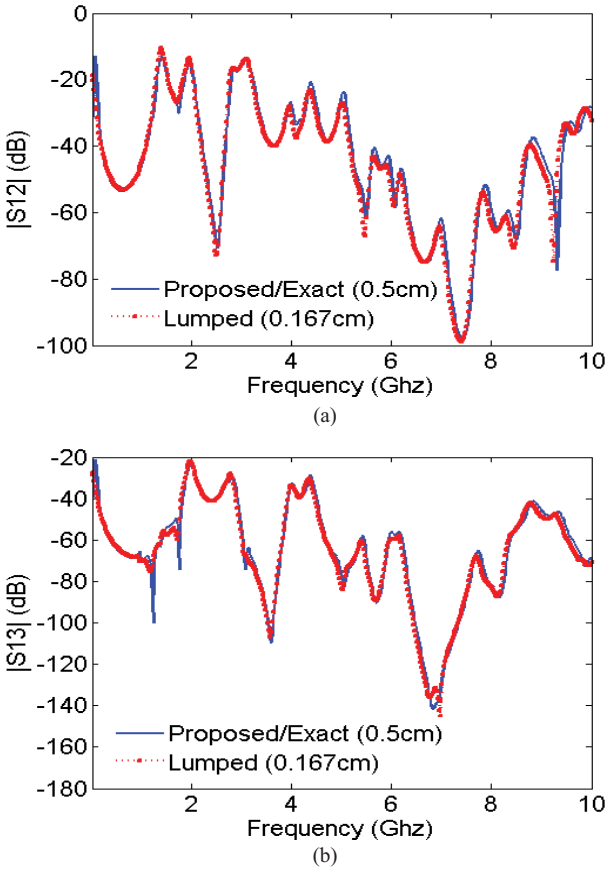

Fig. 8. Comparison of S parameters of Example 1 using proposed model (l = 0.5 cm) and lumped model (l = 0.167 cm). (a) Magnitude of S_{12}. (b) Magnitude of S_{13}.

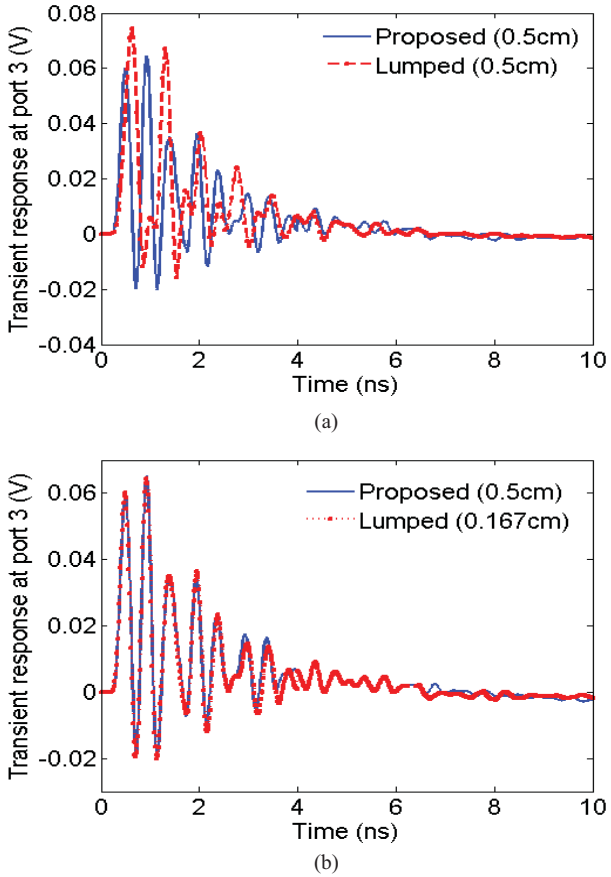

Fig. 9. Comparison of transient response of Example 1 using proposed macromodel (l = 0.5 cm) and lumped model (l = 0.167 cm). (a) Response at Port 2. (b) Response at Port 3.

function as

$$\boldsymbol{Z}(s) \approx \boldsymbol{r}_0^{(z)} + \sum_{i=1}^{N_z} \frac{\boldsymbol{r}_i^{(z)}}{s - p_i^{(z)}}, \quad \boldsymbol{Y}(s) \approx \boldsymbol{r}_0^{(y)} + \sum_{i=1}^{N_y} \frac{\boldsymbol{r}_i^{(y)}}{s - p_i^{(y)}} \tag{16}$$

where $\boldsymbol{r}_0^{(z)}$, $\boldsymbol{r}_0^{(y)}$ are the constant matrices; $\boldsymbol{r}_i^{(z)}$, $\boldsymbol{r}_i^{(y)}$ are the matrix containing the ith residue, $p_i^{(y)}$, $p_i^{(z)}$ are the ith poles and N_z, N_y are the order in the rational approximation of (16). The poles and residue matrices of (16) can be obtained offline for various orders of accuracy while ensuring that the rational approximation is positive real to maintain the passivity of the macromodel [25]. Once the rational functions of (16) are available, the DEPACT uses a matrix rational approximation derived from a closed form Padé representation of the exponential function of $e^{\mathbf{A}(s)/2}$ [32], [33]. Since the discretization of PDNs result in short MTL segments and the delays of these segments ($e^{s\mathbf{B}}$) have been extracted in (13), a Padé order of 1/1 (i.e., $e^x = (1-x/2)^{-1}(1+x/2)$) is sufficient to accurately approximate the exponential matrix of (11) as

$$e^{\boldsymbol{A}(s)/2} \approx \left[\boldsymbol{I} - \frac{\boldsymbol{A}(s)}{4}\right]^{-1} \left[\boldsymbol{I} + \frac{\boldsymbol{A}(s)}{4}\right]. \tag{17}$$

Replacing the rational approximation of (16) in (17), the exponential matrix of (17) can be now be expressed as

$$e^{\boldsymbol{A}(s)/2} = \begin{bmatrix} \boldsymbol{A}_i(s) & \boldsymbol{B}_i(s) \\ \boldsymbol{C}_i(s) & \boldsymbol{D}_i(s) \end{bmatrix} \tag{18}$$

where the $\boldsymbol{A}_i(s), \boldsymbol{B}_i(s), \boldsymbol{C}_i(s)$ and $\boldsymbol{D}_i(s)$ of (18) are expressed in rational form as

$$\mathbf{A}_i(s) \approx \mathbf{a}_0 + \sum_{j=1} \frac{\boldsymbol{a}_j}{s - \tilde{p}_j} \tag{19}$$

$$\boldsymbol{B}_i(s) \approx \boldsymbol{b}_0 + \sum_{j=1} \frac{\boldsymbol{b}_j}{s - \tilde{p}_j} \tag{20}$$

$$\boldsymbol{C}_i(s) \approx \boldsymbol{c}_0 + \sum_{j=1} \frac{\boldsymbol{c}_j}{s - \tilde{p}_j} \tag{21}$$

$$\boldsymbol{D}_i(s) \approx \boldsymbol{d}_0 + \sum_{j=1} \frac{\boldsymbol{d}_j}{s - \tilde{p}_j} \tag{22}$$

and the constant matrices $\boldsymbol{a}_j, \boldsymbol{b}_j, \boldsymbol{c}_j, \boldsymbol{d}_j$ and poles $\tilde{p}_j$ can be obtained from (17). It is observed that the rational approximation of (16) is independent of the discretization of the structure (i.e., line length l) and hence needs to be done only once for a given bandwidth of interest $f_{\max}$. With the knowledge of the rational approximation of (16), the macromodel of (19)–(22) can be obtained in a closed form manner for any arbitrary discretization while maintaining the passivity of the model [25]. It is also appreciated that the macromodel of (19)–(22) can be included in the MNA matrices of the structure for transient analysis using recursive convolution [30] and this does not augment the MNA matrices in comparison to the lumped models, which capture the frequency-dependent effects

TABLE I
COMPARISON OF CPU RUN TIME OF PROPOSED MODEL WITH LUMPED MODEL FOR TRANSIENT ANALYSIS OF EXAMPLE 1

Model	No. of unit cells (length of MTL segment)	CPU time (sec)	RMS error w.r.t. IFFT of exact solution of (11)
Proposed	100 ($l = 0.5$ cm)	60.33	$4.46e^{-3}$
Lumped	100 ($l = 0.5$ cm)	72.35	$109.11e^{-3}$
	400 ($l = 0.25$ cm)	218.20	$50.33e^{-3}$
	900 ($l = 0.167$ cm)	483.60	$6.56e^{-3}$

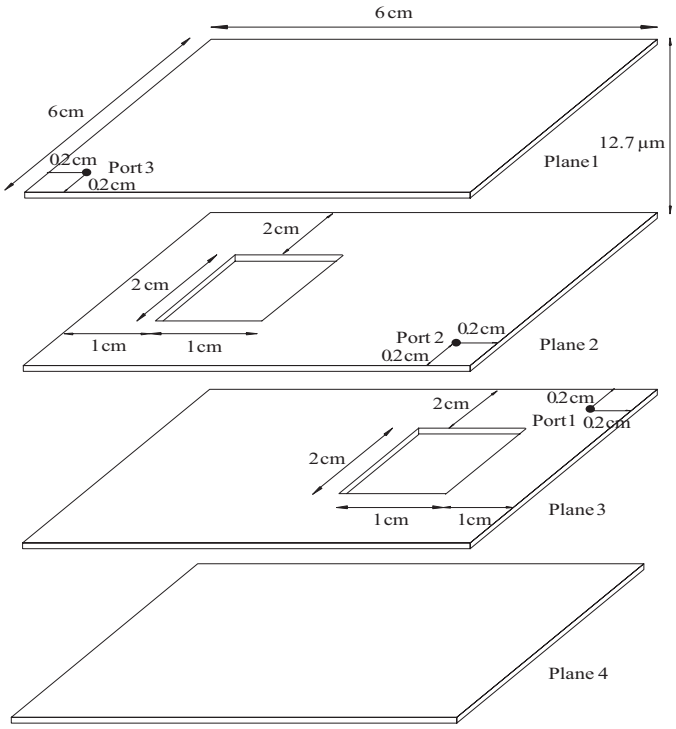

Fig. 10. Test structure for Example 2.

using RL/RC ladders, thereby introducing extra nodes/circuit variables in the MNA matrices [27].

IV. NUMERICAL EXAMPLES

Two examples are presented in this section to demonstrate the validity and efficiency of the proposed algorithm. In this paper, the rational approximation of (16) is obtained using the vector fitting (VF) algorithm [24] on MATLAB 2009b platform and verified to be passive using [25]. For the examples of this section, $N_z = N_y = 4$ in (16) which corresponds to a fourth order RL/RC ladder to capture the skin effect losses and dispersive effects. The proposed macromodel based on DEPACT is compared with the results of the lumped model based on the MFDM [21] (hereafter referred to as the lumped model) and the solution of the Telegrapher's partial differential equation of (11) in frequency domain (hereafter referred to as exact solution) where all models are simulated using HSPICE on an UNIX server (66-GB RAM and 160-GB memory).

Example 1—Irregular Shaped Multilayered PDN: The objective of this example is to compare the accuracy and efficiency of the proposed DEPACT model with the lumped model. For this purpose a six-layered PDN structure as illustrated in Fig. 6 is considered. Each plane of this PDN is 5×5 cm, made of copper of thickness $t = 0.025$ mm and separated from each other by a FR4 dielectric medium ($\varepsilon_r = 4.27$) of thickness $d = 12.7$ μ m. The input port is located at Port 1 on plane 1 (4.5, 4.5) and two output ports are located at Port 2 on plane 3 (0.5, 0.5) and Port 3 on plane 4 (4.5, 0.5) where all the above ports are defined with respect to plane 6. Due to the irregular geometry of the planes 2–5, wraparound currents arising in these planes lead to the coupling of entire multilayered structure.

The three-port S-parameters of the PDN structure of Fig. 6 is extracted using three different methodologies—a reference model based on the exact frequency domain solution of (11) for each MTL segment, the proposed macromodel based on DEPACT and the lumped model. In this example, a cell dimensions of $l = 0.5$ cm is expected to provide sufficiently accurate results for an input signal of rise time T_r =0.2 ns [20], [40]. As a result, for each of the above model the discretization is set to $l = 0.5$ cm. The results of the above analyses are shown in Fig. 7. It is observed that, although the proposed macromodel demonstrates good agreement with the exact solution of (11) over a bandwidth of 0–10 GHz, the lumped model can only match the results up to 4 GHz. The high-frequency errors in Fig. 7 arise due to the inability of the lumped model to capture the distributed effects of the relatively large unit cell. The results of the lumped model can be improved by considering a smaller discretization of the structure. For this example, the maximum cell dimensions allowable for the lumped model to match the results of the proposed macromodel over the entire bandwidth are $l = 0.167$ cm and the corresponding results are illustrated in Fig. 8.

For the transient analysis, an input source modeled as a Norton's equivalent current source with source resistance $R_s = 20\ \Omega$ and having a triangular pulse waveform with rise time T_r =0.2 ns and amplitude 50 mA is placed at Port 1, whereas terminating resistances of $R = 500\ \Omega$ is placed at Ports 2 and 3. The input source mimics the injected SSN and the transient response at Ports 2 and 3 represents the noise coupling due to the wraparound current. The transient response at Ports 2 and 3 using both proposed macromodel and lumped model for the same cell discretization ($l = 0.5$ cm) is shown in Fig. 9(a). When the cell discretization for the lumped model is reduced to $l = 0.167$ cm, the transient response for the lumped model shows better agreement with the two models as shown in Fig. 9(b).

Table I illustrates the computational expense and associated accuracy for the transient analysis using the proposed macromodel and the lumped model. For this purpose, both the above two models are compared with respect to the reference model where an IFFT operation is performed on the exact solution of (11). It is noted that the proposed macromodel is about two orders of magnitude more accurate than the lumped model of same discretization. For this example the proposed macromodel is eight times as efficient as the lumped model for a relative error of both models below $10e^{-3}$.

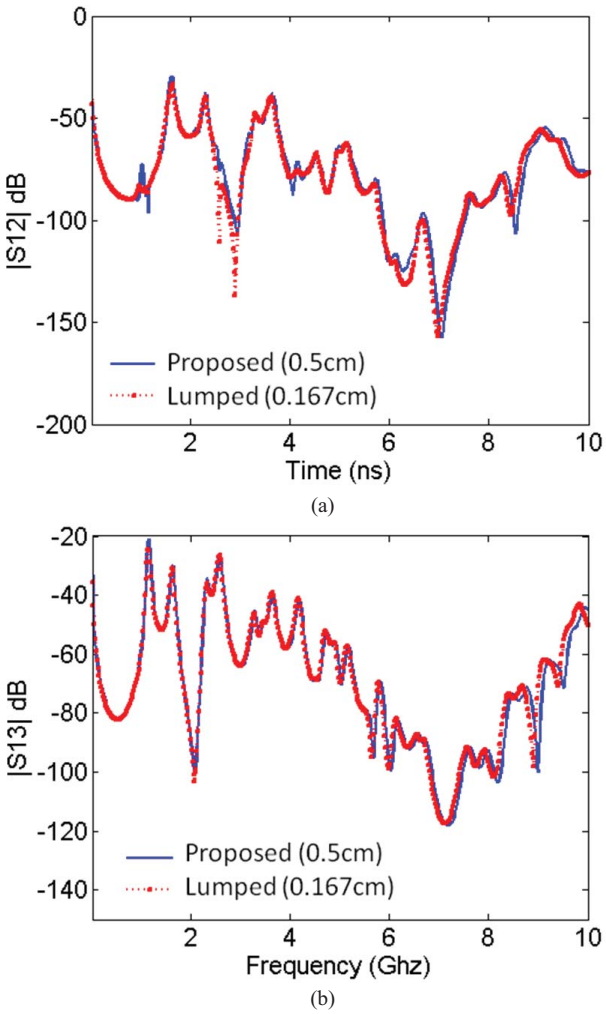

Fig. 11. Comparison of S parameters of Example 2 using proposed model ($l = 0.5$ cm) and lumped model (0.167 cm). (a) Magnitude of S_{12}. (b) Magnitude of S_{13}.

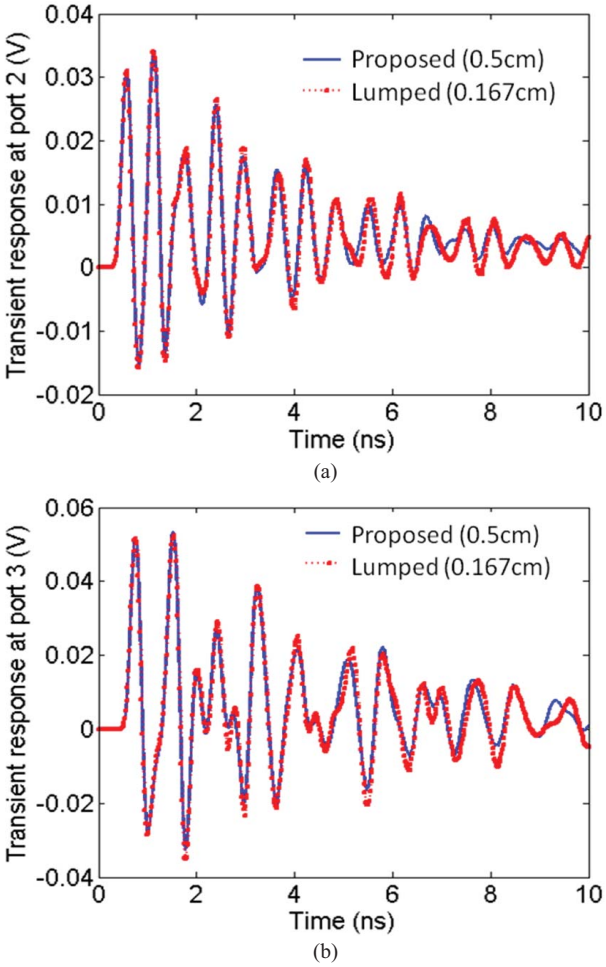

Fig. 12. Comparison of transient response of Example 2 using proposed macromodel ($l = 0.5$ cm) and lumped model (0.167 cm). (a) Response at Port 2. (b) Response at Port 3.

Example 2—Multilayered PDN With Apertures: This example illustrates the EM coupling due to apertures in the multilayered PDN structures. For this purpose, a four-layered PDN structure as illustrated in Fig. 10 is considered. Each plane of this PDN is 6 cm by 6 cm, made of copper of thickness $t = 0.025$ mm and separated from each other by a FR4 dielectric medium ($\varepsilon_r = 4.27$) of thickness $d = 12.7\ \mu$ m. The input port is located at Port plane 1 on plane 3 (5.8, 5.8), and two output ports are located at Port 2 on plane 2 (0.2, 0.2) and Port 3 on plane 1 (5.8, 0.2) where all the above ports are defined with respect to the plane 4. The presence of the apertures on planes 2–3 is responsible for wraparound current leading to the coupling of all four planes.

The three-port S-parameters of the PDN structure of Fig. 10 is extracted using three different methodologies, similar to Example 1. As before, a cell dimensions of $l = 0.5$ cm is expected to yield sufficiently accurate results for an input signal of rise time $T_r = 0.2$ ns [20], [40]. For this example, the maximum cell dimensions allowable for the lumped model to match the results of the proposed macromodel over the entire bandwidth of 0–10 GHz is $l = 0.167$ cm and the corresponding frequency domain results are illustrated in Fig. 11.

For the transient analysis, an input source modeled as a Norton's equivalent current source with source resistance $R_s = 20\ \Omega$ and having a triangular pulse waveform with rise time $T_r = 0.2$ ns and amplitude 50 mA is placed at Port 1 whereas terminating resistances of $R = 500\ \Omega$ is placed at Ports 2 and 3. The input source mimics the injected SSN and the transient response at Ports 2 and 3 represents the noise coupling due to the wraparound current. The transient response at Ports 2 and 3 using both proposed macromodel ($l = 0.5$ cm) and lumped model ($l = 0.167$ cm) is illustrated in Fig. 12. As expected from Fig. 11, both models show good agreement for this particular discretization. However, for this example, the proposed model requires a CPU cost of 30.66 s whereas the lumped model requires 266.92 s. Thus, the proposed macromodel is nearly nine times as fast as the lumped model.

V. Conclusion

In this paper, a MTL modeling approach was presented for achieving accurate macromodels for the analysis of a multilayered PDNs in electronic packages and boards. The key contribution of this paper was in demonstrating that the finite

difference solution of the Helmholtz equation was a simple discretization of the Telegraphers partial differential equation for a mesh of MTL line segments. Based on this result, a more accurate and efficient delay extraction-based macromodel was developed to model the 3-D structure while including the EM coupling between planes in the transverse direction due to wraparound current. Numerical examples illustrated the validity and the efficiency of the proposed macromodel over existing SPICE models.

REFERENCES

[1] E. E. Davidson, "Electrical design of high speed computer package," *IBM J. Res. Develop.*, vol. 26, no. 3, pp. 349–361, May 1982.

[2] R. R. Tummala, E. J. Rymaszewski, and A. G. Klopfenstein, *Microelectronics Packaging Handbook*, Part. I, 2nd ed. New York, USA: Chapman Hall, 1997.

[3] B. Young, *Digital Signal Integrity*, Chapter 11, Englewood Cliffs, N.J., New York, USA: Prentice Hall, 2001.

[4] M. Swaminathan and A. E. Engin, *Power Integrity Modeling and design for Semiconductors and Systems*, Boston, MA, USA: Prentice Hall, 2007.

[5] S. Berghe, F. Olyslager, D. De Zutter, J. De Moerloose, and W. Temmerman, "Study of the ground bounce caused by power plane resonances," *IEEE Trans. Electromagn. Compat.*, vol. 40, no. 2, pp. 111–119, May 1998.

[6] O. Ramahi, V. Subramanian, and B. Archambeault, "A simple finite difference frequency-domain (FDFD) algorithm for analysis of switching noise in printed circuit boards and packages," *IEEE Trans. Adv. Packag.*, vol. 26, no. 2, pp. 191–198, May 2003.

[7] R. Mitra, S. Chebolu, and W. D. Becker, "Efficient modeling of power planes in computer packages using the finite difference time domain method," *IEEE Trans. Microw. Theory Tech.*, vol. 42, no. 9, pp. 1791–1795, Sep. 1994.

[8] T. K. Sarkar, "Accurate modeling of frequency responses of multiple planes in gigahertz packages and board," in *Proc. 9th Topical Meeting Electr. Perform. Electron. Packag.*, Oct. 2000, pp. 59–62.

[9] C. Guo and T. H. Hubing, "Circuit models for power bus structures on printed circuit boards using a hybrid FEM-SPICE method," *IEEE Trans. Adv. Packag.*, vol. 29, no. 3, pp. 441–447, Aug. 2006.

[10] B. Archambeault and A.E. Ruehli, "'Analysis of power/ground-plane EMI decoupling performance using the partial-element equivalent circuit technique," *IEEE Trans. Electromagn. Compat.*, vol. 43, no. 4, pp. 437–445, Nov. 2001.

[11] J. Choi, M. Sung-Hwan, K. Joong-Ho, M. Swaminathan, W. Beyene, and X. Yuan, "Modeling and analysis of power distribution networks for gigabit applications," *IEEE Trans. Mobile Comput.*, vol. 2, no. 4, pp. 299–313, Oct.–Dec. 2003.

[12] N. Na, J. Choi, S. Chun, and M. Swaminathan, "Modeling and transient simulation of planes in electronic packages," *IEEE Trans Adv. Packag.*, vol. 23, no. 3, pp. 340–352, Aug. 2000.

[13] M. A. Schmitt, K. Lam, L. E. Mosley, G. Choksi, and B. K. Bhattacharyya, "Current distribution in power and ground planes of a multilayer pin grid packages," in *Proc. Intl. Electron. Pkg. Soc.*, 1988, pp. 467–475.

[14] W. Becker, B. McCredie, G. Wilkins, and A. Iqbal, "Power distribution modeling of high performance first level computer packages," in *Proc. IEEE 2nd Topical Meeting Electr. Perform. Electron. Packag.*, 1993, pp. 203–205.

[15] H. Kubota, A. Kamo, T. Watanabe, and H. Asai, "Analysis of power/ground planes by PCB simulator with model order reduction technique," in *Proc. 10th Topical Meeting Elect. Perform. Electron. Packag.*, 2001, pp. 77–80.

[16] T. Watanabe and H. Asai, "Model order reduction of electromagnetic systems and RLC circuits for power plane resonance analysis," in *Proc. 12th Topical Meeting Elect. Perform. Electron. Packag.*, 2003, pp. 203–206.

[17] R. Achar, M. S. Nakhla, H. S. Dhindsa, A. R. Sridhar, D. Paul, and N. M. Nakhla, "Parallel and scalable transient simulator for power grids via waveform relaxation (PTS-PWR)," *IEEE Trans. Very Large Scale Integr. (VLSI) Systs.*, vol. 19, no. 2, pp. 319–332, Feb. 2011.

[18] H. H. Wu, J. W. Meyer, K. Lee, and A. Barber, "Accurate power supply and ground plane pair models," *IEEE Trans. Adv. Packag.*, vol. 22, no. 3, pp. 259–266, Aug. 1999.

[19] L. Smith, R. Raymond, and T. Roy, "Power plane SPICE models and simulated performance for materials and geometries," *IEEE Trans. Adv. Packag.*, vol. 24, no. 3, pp. 277–287, Aug. 2001.

[20] S. Roy and A. Dounavis, "Efficient modeling of power/ground planes using delay extraction based transmission lines," *IEEE Trans. Comp. Packag. Manuf. Tech.*, vol. 1, no. 5, pp. 761–771, May 2011.

[21] A. E. Engin, K. Bharath, and M. Swaminathan, "Multilayered finite-difference method (MFDM) for modeling of package and printed circuit board planes," *IEEE Trans. Electromagn. Compat.*, vol. 49, no. 2, pp. 441–447, May 2007.

[22] R. Ito, "Parallel plate slot coupler using 2-D frequency domain transmission line matrix method," in *Proc. 13th Topical Meeting Elect. Perform. Electron. Packag.*, Oct. 2004, pp. 41–44.

[23] Y. Jeong, A. C. W. Lu, L. L. Wai, W. Fan, B. K. Lok, H. Park, and J. Kim, "Hybrid analytical modeling method for split power bus in multilayered package," *IEEE Trans. Electromagn. Compat.*, vol. 48, no. 1, pp. 82–94, Feb. 2006.

[24] B. Gustavsen and A. Semlyen, "Rational approximation of frequency domain responses by vector fitting," *IEEE Trans. Power Del.*, vol. 14, no. 3, pp. 1052–1061, Jul. 1999.

[25] S. Grivet-Talocia, "Passivity enforcement via perturbation of Hamiltonian matrices," *IEEE Trans. Circuit Syst. I*, vol. 51, no. 9, pp. 1755–1769, Sep. 2004.

[26] S. N. Lalgudi, E. Engin, G. Casinovi, and M. Swaminathan, "Accurate transient simulation of interconnect characterized by band-limited data with propagation delay enforcement in a modified nodal analysis framework," *IEEE Trans. Eletromagnetic Compat.*, vol. 50, no. 3, pp. 715–729, Aug. 2008.

[27] A. E. Engin, W. Mathis, W. John, G. Sommer, and H. Reichl, "Closed-form network representations of frequency-dependent RLGC parameters," *Int. J. Circuit Theory Appl.*, vol. 33, pp. 463–485, Nov. 2005.

[28] N. Nakhla, A. Dounavis, R. Achar, and M. S. Nakhla, "DEPACT: Delay extraction-based passive compact transmission-line macromodeling algorithm," *IEEE Trans. Adv. Packag.*, vol. 28, no. 1, pp. 13–23, Feb. 2005.

[29] N. Nakhla, M. S. Nakhla, and R. Achar, "Simplified delay extraction-based passive transmission line macromodeling algorithm," *IEEE Trans. Adv. Packag.*, vol. 33, no. 2, pp. 498–509, May 2010.

[30] S. Lin and E. S. Kuh, "Transient simulation of lossy interconnects based on a recursive convolution formulation," *IEEE Trans. Circuits Syst. I: Fundam. Theory Appl.*, vol. 39, no. 11, pp. 879–892, Nov. 1992.

[31] A. Odabasioglu, M. Celik, and L. T. Pilleggi, "PRIMA: Passive reduced-order interconnect macromodeling algorithm," *IEEE Trans. Comput.-Aided Des. Integr. Circuits Syst.*, vol. 17, no. 8, pp. 645–653, Aug. 1998.

[32] A. Dounavis, R. Achar, and M. Nakhla, "Efficient passive circuit models for distributed networks with frequency-dependent parameters," *IEEE Trans. Adv. Packag.*, vol. 23, no. 8, pp. 382–392, Aug. 2000.

[33] A. Dounavis, R. Achar, and M. Nakhla, "A general class of passive macromodels for lossy multiconductor transmission lines," *IEEE Trans. Microw. Theory Tech.*, vol. 49, no. 10, pp. 1686–1696, Oct. 2001.

[34] A. Cangellaris, S. Pasha, J. Prince, and M. Celik, "A new discrete transmission line model for passive model order reduction and macromodeling of high-speed interconnections," *IEEE Trans. Adv. Packag.*, vol. 22, no. 3, pp. 356–364, Aug. 1999.

[35] Q. Yu, J. M. L. Wang, and E. S. Kuh, "Passive multipoint moment matching model order reduction algorithm on multiport distributed interconnect networks," *IEEE Trans. Circuits Syst. I, Fundam. Theory Appl.*, vol. 46, no. 1, pp. 140–160, Jan. 1999.

[36] E. Gad and M. Nakhla, "Efficient simulation of nonuniform transmission lines using integrated congruence transform," *IEEE Trans. Very Large-Scale Integr. (VLSI) Syst.*, vol. 12, no. 5, pp. 1307–1320, May 2004.

[37] F. Fer, "Resolution de l'equation matricielle par produit infini d'exponentielles matricielles," *Acad. Roy. Belg. Cl. Sci.*, vol. 44, no. 5, pp. 818-829, 1958.

[38] C. R. Paul, *Analysis of Multiconductor Transmission Line*, New York, USA: 2008.

[39] F. H. Branin, "Transient analysis of lossless transmission lines," *Proc. IEEE*, vol. 55, no. 11, pp. 2012–2013, Nov. 1967.

[40] J.-H. Kim and M. Swaminathan, "Modeling of irregular shaped power distribution planes using transmission matrix method," *IEEE Trans. Adv. Packag.*, vol. 24, no. 3, pp. 334–346, Aug. 2001.

Sourajeet Roy (S'11) received the B.Tech. degree in electrical engineering from Sikkim Manipal University, Gangtok, India, in 2006, and the M.E.Sc. degree from Western University, London, ON, Canada, in 2009, where he is currently pursuing the Ph.D. degree with the Department of Electrical and Computer Engineering.

His current research interests include modeling and simulation of high-speed circuits, signal and power integrity analysis of electronic packages, and design and implementation of parallel algorithms.

Mr. Roy was a recipient of the Vice-Chancellors Gold Medal at the undergraduate level in 2006, the Queen Elizabeth II Graduate Scholarship in Science and Technology in 2012, and the Ontario Graduate Scholarship in 2012.

Anestis Dounavis (S'00–M'03) received the B.Eng. degree from McGill University, Montreal, QC, Canada, in 1995, and the M.Sc. and Ph.D. degrees from Carleton University, Ottawa, ON, in 2000 and 2004, respectively, all in electrical engineering.

He is currently an Associate Professor with the Department of Computer and Electrical Engineering, Western University, London, ON. His current research interests include electronic design automation, simulation of high-speed and microwave networks, signal integrity, and numerical algorithms.

Dr. Dounavis was a recipient of the Carleton University Medal for outstanding graduate work at the M.Sc. and Ph.D. levels in 2000 and 2004, respectively, the INTEL Best Student Paper Award at the Electrical Performance of Electronic Packaging Conference in 2003, the Student Researcher of the Year Award from Ottawa Centre for Research and Innovation Futures in 2004, and the University Student Council Teaching Honour Roll Award from the Western University for 2009–2010.